

An Effective Model of HL-60 Differentiation

Ryan Tasseff*, Holly Jensen*, Johanna Congleton†, Andrew Yen†, Jeffrey D. Varner*

*School of Chemical and Biomolecular Engineering, Cornell University, Ithaca, NY 14850 USA †Department of Biomedical Sciences, Cornell University, Ithaca, NY 14850 USA

Abstract—Lessons learned in differentiation models, such as the lineage-uncommitted human myeloblastic cell line HL-60, inform the analysis of more complex programs important to therapeutic applications. In this study, we developed a minimal model of the All-Trans Retinoic Acid (ATRA) differentiation circuit of HL-60. The minimal model encoded the positive feedback between an ATRA-inducible membrane localized signalsome complex and mitogen-activated protein kinase (MAPK) activation. We estimated an ensemble of model parameters using measurements from ATRA-induced HL-60 differentiation, and tested the model in experimentally perturbed HL-60 cells. Bifurcation analysis of this model predicted bistability in ppERK levels as a function of ATRA forcing. A functional consequence of this was the ability to lock the MAPK cascade into a self-sustaining activated state, even after ATRA removal. These simulations were then qualitatively validated with ATRA washout experiments. The minimal model, despite its simplicity, captured the key features of the ATRA response of HL-60 cells such as sustained MAPK activation, the impact of gene deletion and kinase inhibition.

Index Terms—Differentiation, mathematical modeling, bifurcation analysis.

I. INTRODUCTION

Understanding differentiation, the process by which precursor cells become more specialized cell types, is an important challenge. Lessons learned in differentiation models, such as the lineage-uncommitted human myeloblastic cell line HL-60, informs our analysis of more complex programs important to therapeutic applications. HL-60 has been a durable experimental differentiation model since the late 1970's [1]. HL-60 undergoes cell cycle arrest and either myeloid or monocytic differentiation following stimulation. All-Trans Retinoic Acid (ATRA) induces G1/G0-arrest and myeloid differentiation in HL-60 cells, while 1,25-dihydroxy vitamin D₃ induces arrest and monocytic differentiation. Commitment to cell cycle arrest and terminal differentiation requires approximately 48 hr of treatment, during which HL-60 cells undergo two division cycles.

Sustained mitogen-activated protein kinase (MAPK) activation is a defining feature of ATRA-induced HL-60 differentiation. ATRA drives sustained MEK-dependent activation of the RAF/MEK/ERK pathway, leading to arrest and functional differentiation [12]. MEK inhibition results in the loss of ERK and RAF phosphorylation, and the failure to arrest and terminally differentiate [3], [12]. ATRA (and its metabolites) are ligands for the hormone activated nuclear transcription factors retinoic acid receptor (RAR) and retinoid X receptor (RXR) [5]. Activation of RAR and RXR is necessary for

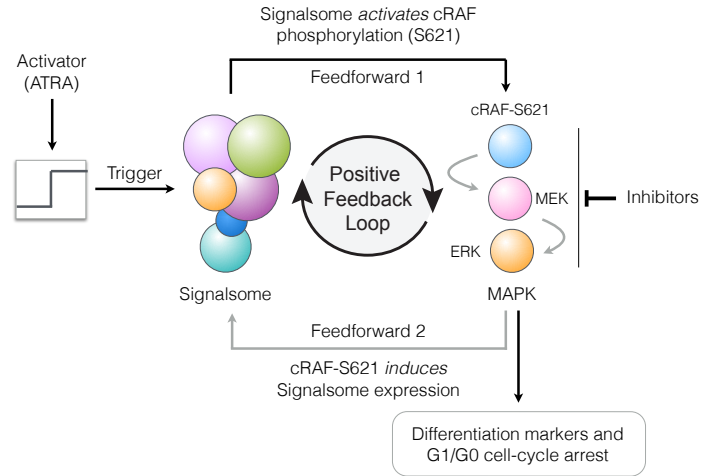


Fig. 1. Schematic of the reduced All-Trans Retinoic Acid (ATRA) differentiation circuit. ATRA activates an upstream Trigger, which promotes the formation of the signalsome complex. The signalsome activates the mitogen-activated protein kinase (MAPK) cascade. MAPK then drives the downstream differentiation program and signalsome formation.

ATRA-induced RAF phosphorylation and MAPK activation [3]. Transcription factor complexes involving RAR and RXR induce the expression of several proteins including the putative heterotrimeric Gq protein-coupled receptor BLR1 [7]. BLR1, identified as an early ATRA (or D3)-inducible gene in HL-60 [11], is necessary for MAPK activation, growth arrest and functional differentiation [7]. Members of the BLR1 transcriptional activator complex, e.g. NFATc3 and CREB, are phosphorylated by ERK, JNK or p38 MAPK family members suggesting positive feedback between BLR1 expression and MAPK activation [10]. BLR1 overexpression enhanced RAF phosphorylation and accelerated terminal differentiation. BLR1 knock-out cells failed to activate RAF or differentiate in the presence of ATRA [8]. Lastly, RAF inhibition reduced BLR1 expression and functional differentiation [8].

Tasseff et al., hypothesized that BLR1-MAPK positive feedback was essential for ATRA-induced sustained MAPK activation, cell cycle arrest and functional differentiation [6]. In this study, we tested this hypothesis by analyzing a minimal model of ATRA-inducible HL-60 differentiation (Fig. 1). The minimal model, composed of five differential equations, encoded the positive feedback between an ATRA-inducible membrane localized signalsome complex and MAPK activation. We estimated an ensemble of model parameters using measurements from ATRA-induced HL-60 differentiation, and tested the model in experimentally perturbed HL-60 cells. The minimal model, despite its relative simplicity, captured the

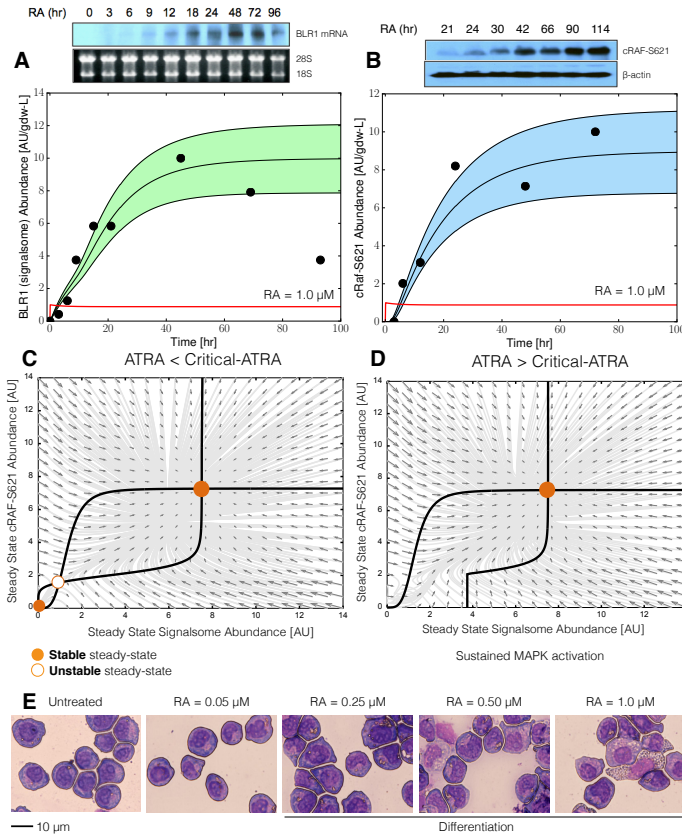


Fig. 2. Model analysis for ATRA-induced HL-60 differentiation. A: BLR1 mRNA versus time following exposure to $1\mu\text{M}$ ATRA at $t = 0$ hr. B: cRAF-S621 versus time following exposure to $1\mu\text{M}$ ATRA at $t = 0$ hr. Points denote experimental measurements, solid lines denote the mean model performance. Shaded regions denote the 99% confidence interval calculated over the parameter ensemble. Qualitative analysis of the effective HL-60 differentiation model. C: Signalsome and cRAF-S621 nullclines for ATRA below the critical threshold. The reduced order model had two stable steady states and a single unstable state in this regime. D: Signalsome and cRAF-S621 nullclines for ATRA above the critical threshold. The reduced order model had only a single stable steady state in this regime. E: HL-60 morphological response to increasing ATRA concentration.

key features of the ATRA response of HL-60 cells such as sustained MAPK activation, the impact of gene deletion and kinase inhibition.

II. RESULTS

The minimal signalsome-MAPK model recapitulated sustained activation following exposure to $1\mu\text{M}$ ATRA (Fig. 2A-B). An ensemble of minimal model parameter sets was estimated by minimizing the difference between simulations and time-series measurements of BLR1 mRNA (signalsome component) and activated cRAF phosphorylated at Serine 621 (cRAF-S621) following the addition of $1\mu\text{M}$ ATRA using particle swarm optimization (PSO). Each particle in the swarm contributed a member to the ensemble of parameter sets. The minimal feedback architecture captured both ATRA-induced BLR1 expression (Fig. 2A) and sustained phosphorylation of cRAF at Serine 621 in a growing population of HL-60 cells (Fig. 2B). However, the minimal architecture failed to capture the decline of BLR1 expression after 48 hr of ATRA exposure,

suggesting additional components were present in the ATRA-induced differentiation circuit.

The minimal signalsome-MAPK feedback circuit was bistable with respect to ATRA forcing (Fig. 2C-D). Bifurcation analysis predicted two stable steady-states and a single unstable state when ATRA was present below a critical threshold (Fig. 2C). In the lower stable state, neither the signalsome nor cRAF-S621 were present. Thus, the differentiation program was deactivated. On the other hand, at the high stable state, both the signalsome and cRAF-S621 were present, indicating sustained activation and differentiation. Interestingly, when ATRA was above the critical threshold, only the activated state was possible (Fig. 2D). Taken together, bifurcation analysis suggested qualitatively different behavior was possible depending upon the degree of ATRA forcing. Below a critical threshold, both deactivated and activated behavior were possible, while above the threshold, only activated behavior was possible. To test these findings, we first identified the ATRA threshold, by exposing HL-60 cells to different ATRA concentrations (Fig. 2E). Morphological changes associated with differentiation were visible for $\text{ATRA} \geq 0.25 \mu\text{M}$, suggesting the critical ATRA threshold was near this concentration.

The minimal model recapitulated molecular perturbations to the ATRA-induced positive feedback circuit (Fig. 3). Self sustaining activation resulted from reinforcing positive feedback between the signalsome and MAPK. Thus, if we inhibited or removed elements from the minimal circuit we expect the signalsome and MAPK signals to decay. We tested this hypothesis by simulating ATRA induced activation in the presence of kinase inhibitors and with key circuit elements removed (Fig. 3). Consistent with previous experimental results using multiple MAPK inhibitors, ATRA activation in the presence of MAPK inhibitors lowered the steady-state value of signalsome (Fig. 3A). BLR1 deletion removed the ability of the circuit to maintain a sustained MAPK response following the withdraw of ATRA (Fig. 3B, gray). On the other hand, in the presence of BLR1, the cRAF-S621 signal was maintained following the withdraw of ATRA, demonstrating the self sustaining nature of the circuit (Fig. 3B, blue). Washout experiments in which cells were exposed to $1.0\mu\text{M}$ ATRA for 24 hr, and then transferred to fresh media without ATRA, confirmed the persistence of the self sustaining activated state for up to 144 hr (Fig. 3C). However, beyond 144 hr the activated MAPK signal (as measured by phosphorylated ERK1/2) decayed. The decreasing MAPK signal indicated additional factors and connections were likely involved in the ATRA circuit beyond the signalsome and MAPK.

III. DISCUSSION

We presented a minimal model of ATRA-inducible differentiation of HL-60 cells. The minimal model, composed of five differential equations, encoded the positive feedback between the ATRA-inducible membrane localized signalsome and the MAPK pathway. We estimated an ensemble of model parameters using measurements of signalsome and MAPK components following ATRA induction in HL-60 using particle swarm optimization. We then tested the model ensemble

using data generated in experimentally perturbed HL-60 cells. The minimal model captured the key features of the ATRA response such as sustained MAPK activation, the impact of gene deletion and kinase inhibition, despite its relative simplicity. Taken together, this study provided further details on sustained MAPK activation, mechanistic insight into cellular memory, and proof-of-concept that a combination of experimental and computational methods is an effective strategy for dissecting complex intracellular signaling programs.

The performance of the minimal ATRA model was impressive given its limited size. However, there were several issues that could be further explored. First, the choice of max/min integration rules or the particular form of the transfer functions could be generalized to include other rule types and functions. Theoretically, an integration rule is a function whose domain is a set of transfer function inputs, and whose range is $v \in [0, 1]$. Thus, integration rules other than max/min could be used, such as the mean or the product, assuming the range of the transfer functions is always $f \in [0, 1]$. Alternative integration rules such as the mean might have different properties which could influence model identification or performance. For example, a mean integration rule would be differentiable, which allows derivative-based optimization approaches to be used. The particular form of the transfer function could also be explored. We choose a Hill-like function because of its prominence in the systems and synthetic biology community. However, the only mathematical requirement for a transfer function is that it map a non-negative continuous or categorical variable into the range $f \in [0, 1]$. Thus, many types of transfer functions are possible.

IV. MATERIALS AND METHODS

Minimal model equations: We modeled the minimal ATRA differentiation circuit using a hybrid approach which integrated ordinary differential equations with logical rules [9]. This approach allowed mechanistic detail, which normally increases the dimension and complexity of the model equations, to be encoded by logical transfer functions, thereby significantly reducing the model dimension. Let the abundance of species i (x_i) in the model be described by:

$$\frac{dx_i}{dt} = \sum_{j=1}^{\mathcal{R}} \sigma_{ij} r_j(\mathbf{x}, \mathbf{k}) - (\mu + k_{d,i}) x_i \quad i = 1, \dots, \mathcal{M} \quad (1)$$

where \mathcal{R} denotes the number of reactions in the model, and \mathcal{M} denotes the number of species in the model. The quantity $r_j(\mathbf{x}, \epsilon, \mathbf{k})$ denotes the rate of reaction j . Typically, reaction j is a non-linear function of biochemical species abundance and unknown kinetic parameters \mathbf{k} ($\mathcal{K} \times 1$). The quantity σ_{ij} denotes the stoichiometric coefficient for species i in reaction j . If $\sigma_{ij} > 0$, species i is produced by reaction j , if $\sigma_{ij} < 0$, species i is consumed by reaction j , while $\sigma_{ij} = 0$ indicates species i is not connected with reaction j . Material balances were subject to the initial conditions $\mathbf{x}(t_0) = \mathbf{x}_0$.

Each reaction rate was written as the product of two terms, a kinetic term (\bar{r}_j) and a control term (v_j):

$$r_j(\mathbf{x}, \epsilon, \mathbf{k}) = \bar{r}_j v_j \quad (2)$$

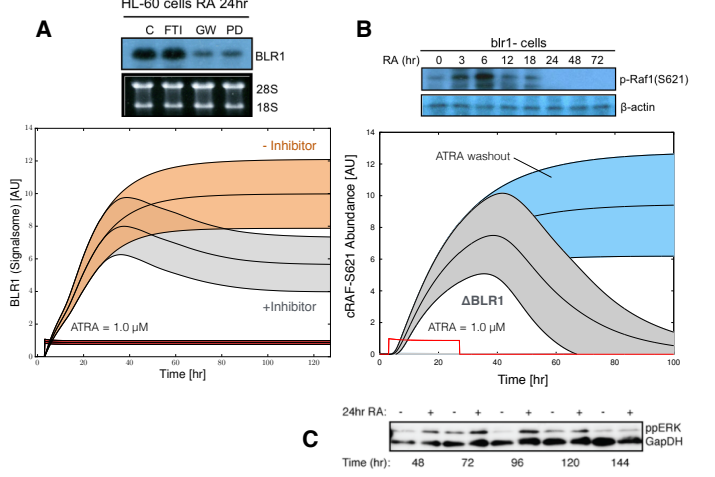


Fig. 3. Model simulation versus experimental data for BLR1 and activated cRAF following ATRA stimulation in HL-60 cells. A: BLR1 mRNA versus time following exposure to $1.0\text{ }\mu\text{M}$ ATRA with and without kinase inhibitor. B: cRAF-S621 versus time following exposure to $1.0\text{ }\mu\text{M}$ ATRA at $t = 3$ hr and removal of ATRA at $t = 24$ hr. Blue region denotes the nominal model, while gray denotes ATRA and BLR1 removal. C: Western blot of phosphorylated ERK1/2 as a function of time in HL-60 cells following exposure to $1.0\text{ }\mu\text{M}$ ATRA at $t = 0$ hr and removal of ATRA at $t = 24$ hr. Points denote experimental measurements. The solid line denotes the mean model performance while the shaded regions denote the 99% confidence interval calculated over the parameter ensemble. Experimental data in panels A and B were reproduced from Wang and Yen [8], data in panel C is reported in this study.

In this study, we used either zero- or first-order kinetics. The control term $0 \leq v_j \leq 1$ depended upon the combination of factors which influenced the activity of species i . For each node, we used a rule-based approach to select from competing control factors. If a node j was influenced by $1, \dots, m$ possible factors, we modeled this relationship as:

$$v_j = \mathcal{I}_j(f_{1j}(\mathcal{Z}), \dots, f_{mj}(\mathcal{Z})) \quad (3)$$

where $0 \leq f_{ij}(\mathcal{Z}) \leq 1$ was a regulatory transfer function that quantified the influence of node i on the activity of node j . The function $\mathcal{I}_j(\cdot)$ denotes an integration rule which maps the output of each of the regulatory transfer functions into the overall control variable for process j . If a process has no modifying factors, $v_j = 1$. While there are many possible forms for $f_{ij}(\mathcal{Z})$, in this study, each regulatory transfer function took the form:

$$f_i(\mathcal{Z}_j, k_{ij}) = k_{ij}^\eta \mathcal{Z}_j^\eta / (1 + k_{ij}^\eta \mathcal{Z}_j^\eta) \quad (4)$$

where \mathcal{Z}_j denotes the abundance of the j factor (e.g., metabolite or protein abundance), and k_{ij} and η are control parameters. The parameter k_{ij} was a gain parameter, while η was a cooperatively parameter. In this study, we used $\mathcal{I}_j \in \{\max, \min\}$ as shown in Wayman et al., [9].

Estimation of model parameters: Model parameters were estimated by minimizing the squared difference between simulations and experimental data taken from ATRA-induced HL-60 cells:

$$E_j(\mathbf{k}) = \sum_{i=1}^{\mathcal{T}_j} \left(\hat{M}_{ij} - \hat{y}_{ij}(\mathbf{k}) \right)^2 + \left(\frac{\mathcal{M}'_{ij} - \max y_{ij}}{\mathcal{M}'_{ij}} \right)^2 \quad (5)$$

The terms $\hat{\mathcal{M}}_{ij}$ and \hat{y}_{ij} denote scaled experimental observations and simulation outputs from training set j . The quantity i denoted the sampled time-index and T_j denoted the number of time points for experiment j . The first term in Eqn. (5) quantified the relative error in the simulation. We used only immunoblot measurements for model training. Thus, we trained the model on the *relative* change between bands within each training data set. The read-out from the training immunoblots was band intensity where we assumed intensity was only loosely proportional to concentration. Suppose we have the intensity for species x at time $\{t_1, t_2, \dots, t_n\}$ in condition j . The scaled-value $\hat{\mathcal{M}}_{ij}$ would then be given by:

$$\hat{\mathcal{M}}_{ij} = \frac{\mathcal{M}_{ij} - \min_i \mathcal{M}_{ij}}{\max_i \mathcal{M}_{ij} - \min_i \mathcal{M}_{ij}} \quad (6)$$

Under this scaling $0 \leq \hat{\mathcal{M}}_{ij} \leq 1$ where $\hat{\mathcal{M}}_{ij} = 0$ describes the lowest intensity band and $\hat{\mathcal{M}}_{ij} = 1$ describes the highest intensity band. A similar scaling was defined for the simulation output. The second-term in the objective function ensured the proper concentration scale was estimated by the model. In this study, we set the highest intensity band to $\mathcal{M}'_{ij} = 10$ [AU] for all simulations. We minimized the total model residual $\sum_j E_j$ using Particle swarm optimization (PSO) [4]. The particle swarm optimization routine was implemented in the Python programming language.

Cell culture and treatment: Human myeloblastic leukemia cells (HL-60 cells) were grown in a humidified atmosphere of 5% CO₂ at 37°C and maintained in RPMI 1640 from Gibco (Carlsbad, CA) supplemented with 5% fetal bovine serum from Hyclone (Logan, UT) and 1x antibiotic/antimicotic (Sigma, St. Louis, MO). Cells were cultured in constant exponential growth as described previously [2]. Experimental cultures were initiated at 0.1×10^6 cells/mL 24 hr prior to 1μM ATRA treatment; if indicated, cells were also treated with GW5074 (2μM) 18 hr before ATRA treatment. For the cell culture washout experiments, HL-60 cells were treated with ATRA for 24 hr, washed 3x with prewarmed serum supplemented culture medium to remove ATRA exposure, and reseeded in ATRA-free media as described. Western blot analysis was performed at incremental time points after removal of ATRA.

Chemicals: All-Trans Retinoic Acid (ATRA) from Sigma-Aldrich (St. Louis, MO) was dissolved in 100% ethanol with a stock concentration of 5mM, and used at a final concentration of 1μM (unless otherwise noted). The Raf inhibitor GW5074 from Sigma-Aldrich (St. Louis, MO) was dissolved in DMSO with a stock concentration of 10mM, and used at a final concentration of 2μM. HL-60 cells were treated with 2μM GW5074 with or without ATRA (1μM) at 0 hr. This GW5074 dosage had a negligible effect on the cell cycle distribution, compared to ATRA treatment alone.

Immunoprecipitation and western blotting: Approximately 1.2×10^7 cells were lysed using 400μL of M-Per lysis buffer from Thermo Scientific (Waltham, MA). Lysates were cleared by centrifugation at 16,950 × g in a micro-centrifuge for 20 min at 4°C. Lysates were pre-cleared using 100μL protein A/G Plus agarose beads from Santa Cruz Biotechnology (Santa Cruz, CA) by inverting overnight at 4°C. Beads were

cleared by centrifugation and total protein concentration was determined by a BCA assay (Thermo Scientific, Waltham, MA). Immunoprecipitations were setup by bringing lysate to a concentration of 1.0g/L in a total volume of 300μL (M-Per buffer was used for dilution). The anti-Raf antibody was added at 3 μL. A negative control with no bait protein was also used to exclude the direct interaction of proteins with the A/G beads. After 1 hr of inversion at 4°C, 20μL of agarose beads was added and samples were left to invert overnight at 4°C. Samples were then washed three times with M-Per buffer by centrifugation. Finally proteins were eluted from agarose beads using a laemmli loading buffer. Eluted proteins were resolved by SDS-PAGE and Western blotting. Total lysate samples were normalized by total protein concentration (20μg per sample) and resolved by SDS-PAGE and Western blotting. Secondary HRP bound antibody was used for visualization. All antibodies were purchased from Cell Signaling (Boston, MA) with the exception of anti-p621 Raf which was purchased from Biosource/Invitrogen (Carlsbad, CA), and anti-pS338 Raf which was purchased from Santa Cruz Biotechnology (Santa Cruz, CA); anti-retinoblastoma from Zymed (South San Francisco, CA); and anti-CK2 from BD Biosciences (San Jose, CA).

REFERENCES

1. T. R. Breitman, S. E. Selonick, and S. J. Collins. Introduction of differentiation of the human promyelocytic leukemia cell line (HL-60) by retinoic acid. *Proc. Natl. Acad. Sci. USA*, 77:2936 – 2940, 1980.
2. S. C. Brooks, S. Kazmer, A. A. Levin, and A. Yen. Myeloid differentiation and retinoblastoma phosphorylation changes in hl-60 cells induced by retinoic acid receptor- and retinoid x receptor-selective retinoic acid analogs. *Blood*, 87(1):227–237, Jan 1996.
3. H. Y. Hong, S. Varvayanis, and A. Yen. Retinoic acid causesmek-dependent raf phosphorylation through raralpha plus rxr activation in hl-60 cells. *Differentiation*, 68(1):55–66, Aug 2001.
4. J Kennedy and R Eberhart. Particle swarm optimization. In *Proceedings of the International Conference on Neural Networks*, pages 1942 – 1948, 1995.
5. D. J. Mangelsdorf, E. S. Ong, J. A. Dyck, and R. M. Evans. Nuclear receptor that identifies a novel retinoic acid response pathway. *Nature*, 345(6272):224–229, May 1990.
6. Ryan Tasseff, Satyaprakash Nayak, Sang Ok Song, Andrew Yen, and Jeffrey D Varner. Modeling and analysis of retinoic acid induced differentiation of uncommitted precursor cells. *Integr Biol*, 3:578 – 591, Mar 2011.
7. J. Wang and A. Yen. A novel retinoic acid-responsive element regulates retinoic acid induced BLR1 expression. *Mol. Cell. Biol.*, 24:2423 – 2443, 2004.
8. Jianrong Wang and Andrew Yen. A mapk-positive feedback mechanism for blr1 signaling propels retinoic acid-triggered differentiation and cell cycle arrest. *J Biol Chem*, 283(7):4375–4386, Feb 2008.
9. Joseph A. Wayman, Adithya Sagar, and Jeffrey D. Varner. Dynamic modeling of cell-free biochemical networks using effective kinetic models. *Processes*, 3(1):138, 2015.
10. Teddy T C Yang, Qiufang Xiong, Herv? Enslen, Roger J Davis, and Chi-Wing Chow. Phosphorylation of nfatc4 by p38 mitogen-activated protein kinases. *Mol Cell Biol*, 22(11):3892–3904, Jun 2002.
11. A. Yen. HL-60 cells as a model of growth control and differentiation - The significance of variant cells. *Hemat. Rev.*, 4:5 – 46, 1990.
12. A. Yen, M. S. Roberson, S. Varvayanis, and A. T. Lee. Retinoic acid induced mitogen-activated protein (map)/extracellular signal-regulated kinase (erk) kinase-dependent map kinase activation needed to elicit hl-60 cell differentiation and growth arrest. *Cancer Res*, 58(14):3163–3172, Jul 1998.